frontiers | Frontiers in Soft Matter

TYPE Original Research
PUBLISHED 12 January 2024
DOI 10.3389/frsfm.2024.1340744

OPEN ACCESS

EDITED BY
Payman Jalali,
Lappeenranta University of Technology, Finland

REVIEWED BY
Dong Wang,
Yale University, United States
Hu Zheng,
Tongji University, China

*CORRESPONDENCE
C. Manuel Carlevaro,
manuel@iflysib.unlp.edu.ar

RECEIVED 18 November 2023
ACCEPTED 02 January 2024
PUBLISHED 12 January 2024

CITATION
Carlevaro CM, Kozlowski R and Pugnaloni LA (2024), Flow rate in 2D silo discharge of binary granular mixtures: the role of ordering in monosized systems.
Front. Soft Matter 4:1340744.
doi: 10.3389/frsfm.2024.1340744

Flow rate in 2D silo discharge of binary granular mixtures: the role of ordering in monosized systems

C. Manuel Carlevaro[1]*, Ryan Kozlowski[2] and Luis A. Pugnaloni[3]

[1]Instituto de Física de Líquidos y Sistemas Biológicos, CONICET–Universidad Nacional de La Plata, and Departamento de Ingeniería Mecánica, Facultad Regional La Plata, Universidad Tecnológica Nacional, La Plata, Argentina, [2]Physics Department, College of the Holy Cross, Worcester, MA, United States, [3]Departamento de Física, Facultad de Ciencias Exactas y Naturales, Universidad Nacional de La Pampa, CONICET, Santa Rosa, Argentina

A long-standing debate regarding the dynamics of silo discharge revolves around the use of mono-dispersed circular or spherical grains in simplified two-dimensional models. It is well-known that granular systems composed of particles of the same size can generate crystal or quasi-crystal domains with specific structural and dynamic behaviors. Can this ordering affect the flow rate to an extent that monosized systems cannot be good models for realistic materials? In this work, we present simulations of the discharge of two-dimensional silos filled with binary mixtures of circular grains that conserve the same mean particle size. We address the question of how ordering affects the mass flow rate, in particular considering the limit of mono-sized systems. We find that the typical hexagonal order observed does not affect the flow rate significantly. However, the flow rate does exhibit a weak, nonmonotonic dependence on packing bidispersity that correlates with changes in the outpouring speed of grains in the vicinity of the orifice.

KEYWORDS

granular matter, silo discharge, bidispersity, ordering, flow rate

1 Introduction

In many studies of soft materials, model systems (in the laboratory or *in silico*) are built using monosized entities. Such systems are prone to structural ordering (An et al., 2011). This is so for bubbles (which form foams), colloidal particles (which form gels), cells (which form tissues), and grains (which form bulk solids) alike. Ordering is particularly evident in two-dimensional (2D) systems (Dickinson et al., 1989). In conventional solids, ordering influences strength and deformation under shear; in granular systems, ordering generally increases packing fraction and creates well-defined failure planes under shear. At the same time, the apparent ordering of grains in a granular packing does not correspond to well-defined ordering of contacts and forces between grains. As discussed by Duran (Sands, 2000), a "stack of cannon balls" may look like a very ordered geometrical arrangement. However, if the balls are rigid, not all neighboring balls need to be in contact to have a stable stack since the isostatic point is achieved with only four contacts per particle. There are thus many different contact configurations compatible with a given ordered arrangement (Grindlay and Opie, 1995); geometrical ordering does not imply ordering at the contact level, and by extension, the transmission of forces (Radjaï et al., 1996; Geng et al., 2003).

Since contacts are responsible for the transmission of forces and ultimately for the resulting dynamics of the system, it is natural to wonder if geometrical ordering–that is,

ordering of particle positions which is visible to the naked eye–is at all meaningful to the flow of grains beyond the obvious effect on packing fraction. Recently, attention has been paid to the ordered domains during flow (Cervantes-Álvarez et al., 2023). These authors consider a monosized system of disks in a quasi-2D experiment and identify ordered domains that compete during discharge. The main objective of this work was to identify some signature in the dynamics of the ordered domains that may serve as precursors to clogging; the emphasis was not on the discharge rate of grains between clogs.

Prompted by the concern that clearly visible ordering in monosized systems may provide results that are not representative of more realistic situations, researchers tend to implement strategies to prevent ordering, typically by introducing some degree of polydispersity to the size of the components of the material (Tsuchikusa et al., 2023). There are many open questions around this approach, however. How much polydispersity is needed to eliminate ordering? Does ordering *need* to be eliminated fully? Is polydispersity affecting the results in ways not related to ordering (e.g., size segregation (Gray, 2018))?

The mass flow rate W of a discharging silo is mostly independent of the height of the granular column in the silo and is well-described by the Beverloo correlation (Beverloo et al., 1961). In a 2D system this is

$$W = C\rho_b\sqrt{g}\left(D - k\bar{d}\right)^{3/2}, \tag{1}$$

where D is the length of the orifice, $\bar{d}$ is the mean size of the grains, g is the acceleration of gravity, and ρ_b is the 2D bulk density of the granular material in the silo. The non-dimensional constants C and k are usually determined by fitting available data and vary with properties such as particle shape and particle-particle friction. For disks with friction coefficients above 0.3 it is found that $k \approx 2.0$ and $C \approx 1.5$ (Aguirre et al., 2010; Goldberg et al., 2015; Tang and Behringer, 2016). The 2D bulk density is estimated as the bulk packing fraction, roughly 0.8 in frictional random packings, multiplied by the 2D material density.

The discharge of monosized disks has been considered in a number of experimental and simulation studies (Sakaguchi et al., 1993; Langston et al., 1995; Mankoc et al., 2007; Aguirre et al., 2010; Goldberg et al., 2015; Tang and Behringer, 2016; Ashour et al., 2017; Cervantes-Álvarez et al., 2023). In all cases the Beverloo scaling with the 3/2 power of the orifice size has been confirmed. The Beverloo exponent remains the same for polydisperse systems (Zhou et al., 2015; Madrid et al., 2017; Reddy et al., 2021; Anyam and Anki Reddy, 2022) and even for non-circular particles (Liu et al., 2014; Goldberg et al., 2015; Börzsönyi et al., 2016; Gao et al., 2023), with one known exception being elongated grains in narrow silos that may display a flow rate which increases as the silo discharges (Pongó et al., 2022).

The flow of polydisperse mixtures has also been studied, though not in connection with the state of ordering. Zhou et al. (2015) considered the discharge of 2D binary mixtures of disks using Discrete Element Method (DEM) simulations. As other authors have done in 3D experiments and simulations (Artega and Tüzün, 1990; Humby et al., 1998; Benyamine et al., 2014; Madrid et al., 2017), these authors consider the change in flow rate when fine grains are added into the mixture. Naturally, ordering of the initially monosized system has to be altered by the addition of fine grains. However, since the mean particle size in the mixtures is not kept constant when fine grains are added, the differences in the flow rate cannot be directly attributed to a change in ordering but mainly to the effective reduction of the mean particle size. More recently, Jacobs-Capdeville et al. (2023) studied the discharge of log-normal polydisperse systems of spheres in 3D silos. In this case, the authors varied the spread of the particle sizes but held the median particle diameter fixed, an approach that inspires the current work as a way to decouple the effects of ordering from the effect of mean particle size $\bar{d}$ on the mass flow rate. However, these authors did not investigate the role of ordering in their polydisperse packings and did not focus on small perturbations to the system's dispersity away from monodispersity, instead varying the polydispersity in large steps.

In this work we study the flow rate of 2D binary systems of disks discharging from a rectangular flat-bottom silo, varying bidispersity with fixed mean particle size in order to directly isolate the effects that spatial ordering of particles in the silo has on the outpouring rate. The limiting case of monosized disks presents clear ordered regions. To consider the effect of such ordering, we simulate binary mixtures with the same mean particle size as the monosized reference system; experiments varying dispersity in such a well-controlled manner are not as feasible as computational simulations. We vary the size dispersion within a narrow range in fine increments

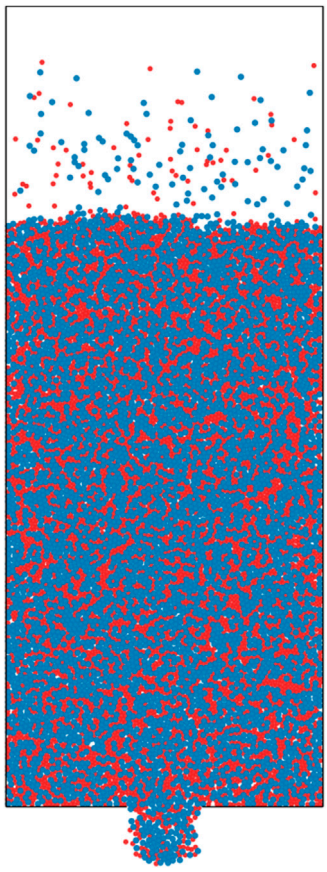

FIGURE 1
Snapshot of a simulation with a $\alpha = 1.31$ binary mixture composed of 5,000 large ($d_L = 1.1239$, blue) and 5,000 small ($d_S = 0.8584$, red), disks. The exiting grains are re-injected at the top at random locations above the free surface in the silo.

in order to observe the flow rate with dispersity as the system smoothly varies from a highly ordered state to a disordered, liquid-like state. We use the Q_6 bond order parameter (Steinhardt et al., 1983) to characterize ordering and show that there exists a nonmonotonic correlation with the flow rate. We then measure the density and velocity profiles along the orifice to evaluate if the origin of our observed changes in the flow rate are connected to packing fraction–another indicator of spatial ordering in granular systems–or changes in the outpouring velocity of grains at the orifice.

2 Simulations

We simulate the discharge of disks from a 2D rectangular silo using a nonsmooth rigid body DEM implemented with the Box2D library (Catto, 2005). A typical snapshot of our simulation is presented in Figure 1. For a monosized system, disks have diameter d and mass m, and the discharge is driven by the acceleration of gravity g pointing in the downward direction. The silo has dimensions of $180d$ in height and $71d$ in width, with an exit hole of diameter $D = 16.9\ d$ located at the center of the base. (While we primarily focus on this large orifice size in the analysis to follow, in Section 3.4 we include results for a much smaller orifice in order to demonstrate the robustness of our findings with orifice size.) For binary mixtures, we introduce in the silo two types of disks: N_L large disks with a diameter of d_L and N_S small disks with a diameter of d_S. We define the size ratio of the packing as $\alpha = d_L/d_S$. The mass of a grain $m_{S,L}$ is proportional to its area, and the area density for both species is set to $4m/(\pi d^2) = 4/\pi$. In the rest of the paper we will use d and m for the monosized system as unit length and unit mass, respectively. The friction and restitution coefficients are the same for the interaction between particles (regardless of their species) and between particles and walls, with values of $\mu = 0.5$ for friction and $\epsilon = 0.1$ for restitution.

The Box2D library employs a constraint solver to handle the dynamics of interacting rigid bodies (Catto, 2005). Box2D is an implementation of a nonsmooth DEM (Moreau, 1988), in which the contact between particles is only defined by a restitution coefficient and friction coefficient instead of a force law, and the particles are considered to be infinitely stiff. In our simulations, we perform a maximum of 60 iterations at each time step to resolve contact dynamics between particles using a Lagrange multiplier scheme. The equations of motion are then advanced (with a time step of $0.01\sqrt{d/g}$) using a symplectic Euler algorithm, which takes into account solid friction based on the Coulomb criterion. Box2D has been used previously to successfully study a range of processes in granular materials such as stick-slip dynamics (Carlevaro et al., 2020), silo discharge of polygonal grains (Goldberg et al., 2015), tapping (Carlevaro and Pugnaloni, 2011), and soil mechanics (Pytlos et al., 2015).

In a single trial, the grains are poured into the silo with the orifice plugged, and the system is allowed to settle until all grains come to rest. The system is defined to be at rest once every grain's translational speed drops below a threshold of $0.01d\sqrt{g/d}$ and angular speed drops below a threshold of $(0.035\ \text{rad})\sqrt{d/g}$. Then, the exit orifice is opened and grains begin to flow out of the silo. The grains that have exited the silo and fallen a vertical distance $12d$ below the orifice plane are re-injected to the top of the silo at random locations in order to maintain a stationary flow rate. The time step at which the centroid of any given particle crosses the orifice line is recorded, and these data are used to calculate the discharged mass time series. Additionally, particle positions and velocities are saved every 1,000 time steps ($10\sqrt{d/g}$, during which roughly 700 particles are discharged) to sample the steady-state particle dynamics as well as structural properties like packing fraction and Q_6. We ensure that steady-state dynamics are achieved before analyzing particle-scale data by waiting $10\sqrt{d/g}$ from the time the orifice is unplugged. In any given realization about 15,000 particles flow out before we end the simulation.

In order to make the flow rate of different binary mixtures (as well as the monosized system) comparable, we keep the mean particle diameter $\bar{d}$ the same, with minor variations due to the discrete nature of the number of grains, in all simulated systems. If the mean particle size changes, we would expect a change in the flow rate based on the Beverloo scaling (Eq. 1) (Beverloo et al., 1961) due to the empty annulus correction term $-k\bar{d}$. Thus, by keeping $\bar{d}$ constant, changes of the flow rate that may occur when varying size dispersion can be attributed to other effects, such as ordering. For binary systems, we use $\bar{d} = d_{10} = (N_L d_L + N_S d_S)/(N_L + N_S)$, weighting based on the relative number of particles of each species (Allen, 2013). (Of course, other definitions are possible, such as weighting based on mass (i.e., d_{32} (Allen, 2013)) instead of particle number. We will revisit this point in the following section.) If we fix $\bar{d}$ and $N = N_L + N_S$, then two free parameters remain (say, N_L and d_L). In order to vary just a single free parameter we consider two alternative additional constraints:

- **Case I** ($N_L = N_S$)**:** In this case we set the number of grains of each species the same. The total mass of each species varies and depends on the selected value of the free parameter (d_L). Table 1 summarizes the set of simulations that were run for this case.
- **Case II** ($M_L = M_S$)**:** In this case we set the total mass of each species ($M_i = N_i \pi d_i^2/4$, with i = S or L) equal. The number of grains of each species varies and depends on the selected value of the free parameter (d_L). Table 2 summarizes the corresponding set of simulations.

We have run simulations of the binary mixtures listed in Tables 1, 2 corresponding to Cases I and II keeping $\bar{d} = 2\bar{r} \approx 1.0$. Note that due to the discrete number of particles, the actual mean particle diameter is not always exactly 1.0. We keep the variation of $\bar{d}$ from 1.0 less than 3.4% across all trials. For each mixture we run 20 realizations of the discharge with different random initial positions of the particles and report mean values over realizations and fluctuations defined by the corresponding standard deviations.

3 Results

3.1 Ordering

To quantify the order in the system we use the Q_6 bond order parameter, which characterize the local order around a given particle (Steinhardt et al., 1983). For a grain, the bond order parameter can

TABLE 1 Set of parameters of the mixtures prepared for simulations of Case I, i.e., $N_L = N_S$. The diameter d_i of each species and the mean diameter $\bar{d} = d_{10}$ are listed along with the size ratio α and the number N_i of grains and total mass M_i of each species.

Case I	d_L	d_S	$\bar{d} = d_{10}$	α	N_L	N_S	M_L	M_S
01	1.0000	1.0000	1.0000	1.0000	5,000	5,000	5,000.0000	5,000.0000
02	1.0130	0.9868	1.0000	1.0266	5,000	5,000	5,131.5744	4,868.4173
03	1.0260	0.9734	0.9996	1.0540	5,000	5,000	5,263.1543	4,736.8370
04	1.0388	0.9598	0.9992	1.0823	5,000	5,000	5,394.7377	4,605.2548
05	1.0514	0.9460	0.9986	1.1114	5,000	5,000	5,526.3056	4,473.6908
06	1.0638	0.9318	0.9978	1.1417	5,000	5,000	5,657.9054	4,342.1135
07	1.0760	0.9176	0.9968	1.1726	5,000	5,000	5,789.4826	4,210.5177
08	1.0882	0.9032	0.9958	1.2048	5,000	5,000	5,921.0485	4,078.9415
09	1.1002	0.8886	0.9944	1.2381	5,000	5,000	6,052.6403	3,947.3745
10	1.1122	0.8736	0.9928	1.2731	5,000	5,000	6,184.2102	3,815.7974
11	1.1240	0.8584	0.9912	1.3094	5,000	5,000	6,315.7785	3,684.2185
12	1.1356	0.8430	0.9892	1.3471	5,000	5,000	6,447.3690	3,552.6381
13	1.1470	0.8272	0.9872	1.3866	5,000	5,000	6,578.9397	3,421.0510
14	1.1584	0.8112	0.9848	1.4280	5,000	5,000	6,710.5186	3,289.4809
15	1.1698	0.7948	0.9822	1.4718	5,000	5,000	6,842.1134	3,157.8994
16	1.1810	0.7780	0.9794	1.5180	5,000	5,000	6,973.6869	3,026.3111
17	1.1920	0.7608	0.9764	1.5668	5,000	5,000	7,105.2736	2,894.7375
18	1.2030	0.7434	0.9732	1.6182	5,000	5,000	7,236.8390	2,763.1583
19	1.2140	0.7254	0.9698	1.6736	5,000	5,000	7,368.4216	2,631.5771
20	1.2248	0.7072	0.9660	1.7319	5,000	5,000	7,499.9893	2,499.9945

be defined either through the contact vectors (the vectors from its center to each contact with its touching neighbors) or through the nearest neighbor (NN) vectors (the vectors from the particle center to the center of each nearest neighbor, irrespective of whether the particles touch). As we mentioned in Section 1, the ordering that usually concerns researchers is appreciated by naked eye in the systems of interest and does not take into account the real contacts. Therefore, we use the NN vectors for the calculation of Q_6. For any given particle with NN vectors $\mathbf{r}$, Q_6 is defined as

$$Q_6 = \left[\frac{4\pi}{13}\sum_{m=-6}^{6}|\bar{Q}_{6,m}|^2\right]^{1/2}. \quad (2)$$

$\bar{Q}_{6,m}$ is the mean over all branch vectors $\mathbf{r}$ of the spherical harmonic $Q_{6,m}(\mathbf{r}) = Y_{6,m}(\theta(\mathbf{r}), \phi(\mathbf{r}))$, with θ and ϕ the Euler angles of $\mathbf{r}$. For a 2D system, $\theta = \pi/2$.

Figure 2A shows a snapshot from one of the monosized simulations with particles colored according to their Q_6 value, as calculated from Eq. 2. This snapshot shows large regions with the typical, clearly visible hexagonal order observed in such systems. The probability distribution function (PDF) of Q_6 taken over all particles in this snapshot is shown in Figure 2B. The peak at around 0.75 correspond to the large number of particles with neighbors in hexagonal arrangement: a hexagonal arrangement yields $Q_6 \approx 0.740829$ (Steinhardt et al., 1983).

In Figure 3 we show some snapshots of monosized and binary systems during the steady state of the discharge with particles colored according to their Q_6 values. Monodisperse systems show clear ordered regions, especially at the stagnant zones at each side of the orifice and upstream away from the orifice. Close to the orifice, the system needs to dilate to be able to flow, and this leads to disorder. For binary systems, the ordering is significantly reduced: the larger the particle size ratio, the less order is observed. The PDFs of Q_6 for each mixture simulated are shown in Figure 4. These PDFs are built from the set of snapshots taken during the simulations in the steady-state discharge. For α close to one, the PDF displays a clear peak at $Q_6 \approx 0.74$ that corresponds to a hexagonal arrangement of the neighbors (Steinhardt et al., 1983). As α increases, this peak drops quickly and lower Q_6 values are populated, indicating a loss of hexagonal order in the bulk of the material.

To quantify ordering globally, we measure the height of the peak of the Q_6 PDF at ≈ 0.74. In Figure 5 we plot the peak height as a function of α, which demonstrates that a relatively small size dispersion ($\alpha > 1.2$) suffices to significantly reduce the strong hexagonal ordering observed in a monosized system. Interestingly, ordering is affected in the same way for a given α regardless of whether the number of particles in each species is fixed (Case I) or the mass of each species is fixed (Case II), suggesting that the size ratio is more significant than relative composition in determining ordering.

TABLE 2 Set of parameters of the mixtures prepared for simulations of Case II, i.e., $M_L = M_S$. The diameter d_i of each species and the mean diameter $\bar{d} = d_{10}$ are listed along with the size ratio α and the number N_i of grains and total mass M_i of each species.

Case II	d_L	d_S	$\bar{d} = d_{10}$	α	N_L	N_S	M_L	M_S
01	1.0000	1.0000	1.0000	1.0000	5,000	5,000	5,000.0000	5,000.0000
02	1.0130	0.9874	1.0000	1.0259	4,872	5,128	5,000.2105	4,999.8000
03	1.0260	0.9760	0.9996	1.0512	4,750	5,250	5,000.0000	5,000.0000
04	1.0388	0.9654	0.9994	1.0760	4,634	5,366	4,999.8421	5,000.1364
05	1.0514	0.9556	0.9988	1.1003	4,524	5,476	5,000.2105	4,999.8261
06	1.0638	0.9464	0.9984	1.1240	4,419	5,581	5,000.4474	4,999.6458
07	1.0760	0.9380	0.9976	1.1471	4,318	5,682	4,999.7895	5,000.1600
08	1.0882	0.9302	0.9970	1.1699	4,222	5,778	4,999.7368	5,000.1923
09	1.1002	0.9230	0.9962	1.1920	4,130	5,870	4,999.4737	5,000.3704
10	1.1122	0.9162	0.9954	1.2139	4,043	5,957	5,000.5526	4,999.6250
11	1.1240	0.9098	0.9944	1.2354	3,958	6,042	4,999.5789	5,000.2759
12	1.1356	0.9036	0.9936	1.2568	3,878	6,122	5,000.5789	4,999.6333
13	1.1470	0.8980	0.9926	1.2773	3,800	6,200	5,000.0000	5,000.0000
14	1.1584	0.8926	0.9916	1.2978	3,725	6,275	4,999.3421	5,000.3906
15	1.1698	0.8876	0.9908	1.3179	3,654	6,346	5,000.2105	4,999.8788
16	1.1810	0.8828	0.9898	1.3378	3,585	6,415	5,000.1316	4,999.9265
17	1.1920	0.8784	0.9888	1.3570	3,519	6,481	5,000.6842	4,999.6286
18	1.2030	0.8740	0.9876	1.3764	3,455	6,545	5,000.6579	4,999.6528
19	1.2140	0.8700	0.9866	1.3954	3,393	6,607	5,000.2105	4,999.8919
20	1.2248	0.8660	0.9856	1.4143	3,333	6,667	4,999.5000	5,000.2500

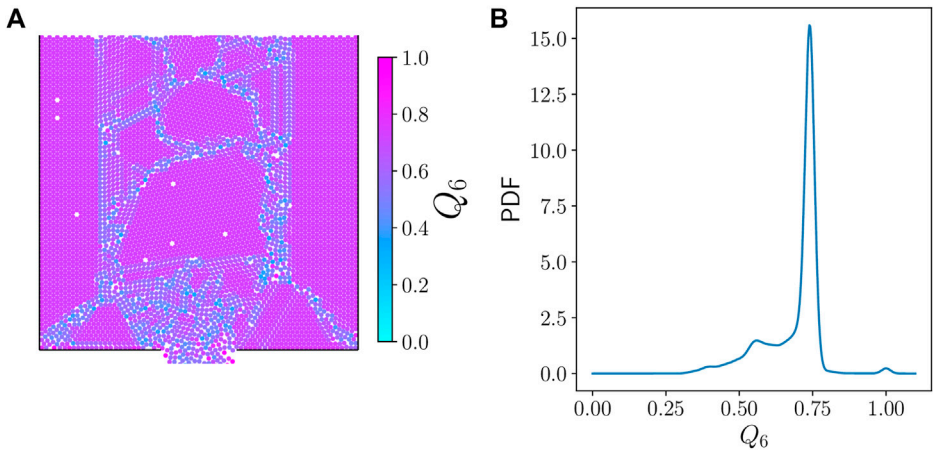

FIGURE 2
(A) Snapshot of a simulation of 10,000 disks of the same diameter d. Particles are colored according to their Q_6 bond order parameters. **(B)** Probability distribution function (PDF) of Q_6 in the snapshot shown in part a.

3.2 Flow rate and mean particle diameter

The mass flow rate is measured by plotting the mass of grains that crosses the orifice plane as a function of time, as shown in Figure 6, and fitting a straight line to the portion of the curve where the flow rate is constant to avoid the initial transient.

In Figure 7 we show the total mass flow rate W as a function of α for cases I and II, determined both from the mass of grains

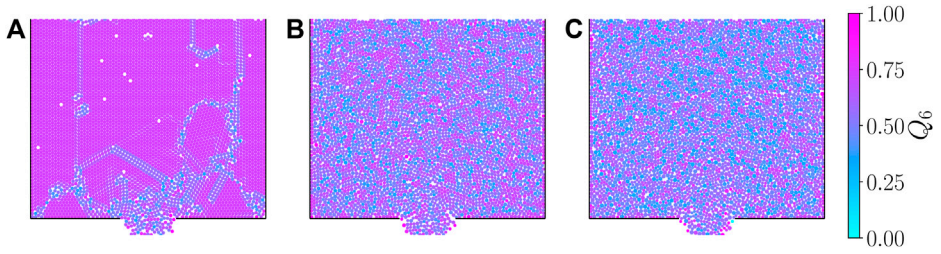

FIGURE 3
Snapshots of simulations with binary mixtures of same $\bar{d}$ for different size ratios: **(A)** $\alpha = 1.0$ (monosized), **(B)** $\alpha = 1.214$ (Case II C-09) and **(C)** $\alpha = 1.414$ (Case II C-19). Particles are colored according to their Q_6 values.

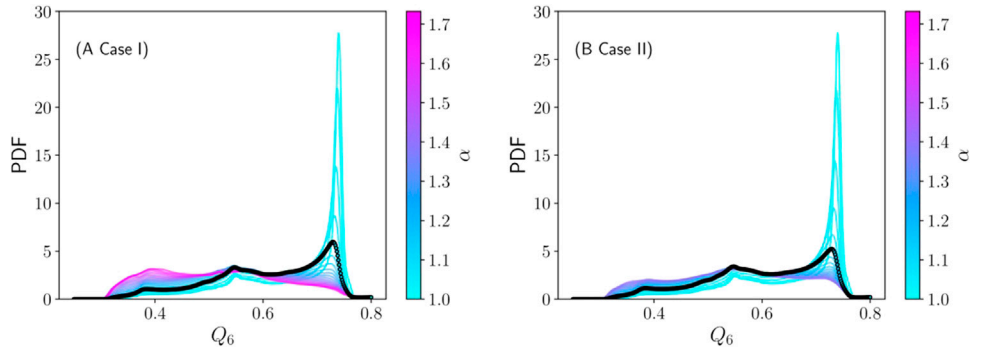

FIGURE 4
PDF of Q_6 for mixtures with $N_L = N_S$ (A, Case I) and $M_L = M_S$ (B, Case II) for varying α (see color scale). The thick black line corresponds to the α-value at which the maximum flow rate is observed (see Figure 7).

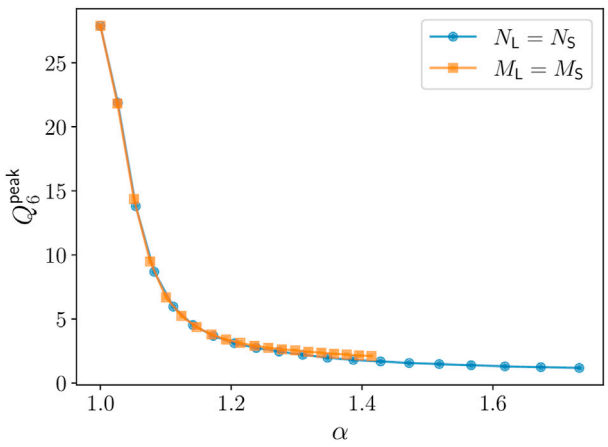

FIGURE 5
Height Q_6^{peak} of the peak at $Q_6 \approx 0.74$ of the PDF of Q_6 as a function of α for the two considered cases.

crossing the orifice over time and from spatial analysis, as described in Section 3. Beyond run-to-run fluctuations, W clearly varies nonmonotonically with α despite the mean particle size being roughly the same in all mixtures. Given that hexagonal order decays monotonically with α, we therefore cannot conclude that there is a correlation between ordering and flow rate. The variation of W is about 8%, which is discernible considering the error bars (standard deviation over realizations) and beyond the variations in mean particle size from 1.0 discussed in Section 2. Monosized (or close to monosized) systems present the lowest flow rate and a maximum is observed at $\alpha \approx 1.15$. Interestingly, for the largest size ratios the flow rate cannot be distinguished from that of the monosized system considering the fluctuations among realizations. It is important to note, however, that the monosized system presents larger run-to-run fluctuations in comparison with bidisperse mixtures with $\alpha > 1.2$.

Jacobs-Capdeville et al. (2023) has shown a monotonic variation for constant median particle size as the width of the log-normal particle distribution (in the log-normal distribution the size ratio is defined by the sizes of the 10th and 90th percentiles of the distribution) is increased for 3D silos. However, the size ratios investigated ($2.0 < \alpha < 8.0$) in their study are outside the range we consider here, which are closer to the monodisperse limit. (And, of course, we study a 2D system.) Interestingly, in Ref. (Jacobs-Capdeville et al., 2023). the flow rate increases with α if the size distribution is particle number-based (equivalent to our Case I) but decreases with α if it is particle volume-based (equivalent to our Case II).

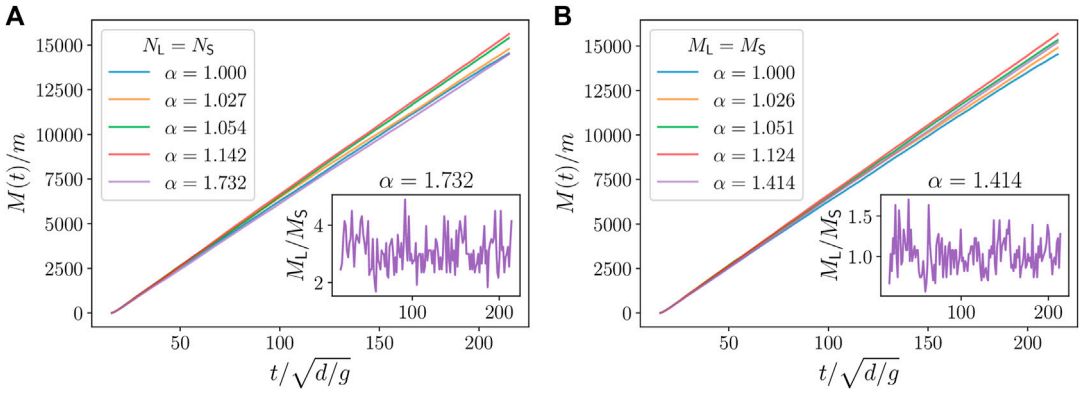

FIGURE 6
Discharged mass as a function of time for different α for some sample simulations of Case I **(A)** and Case II **(B)**, with the mixtures as defined in Tables 1, 2, respectively. Inset: "Instantaneous" mass ratio M_L/M_S discharged as a function of time for the largest value of α studied in each case. The instantaneous mass ratio is sampled over short intervals of time during which roughly 100 particles flow out.

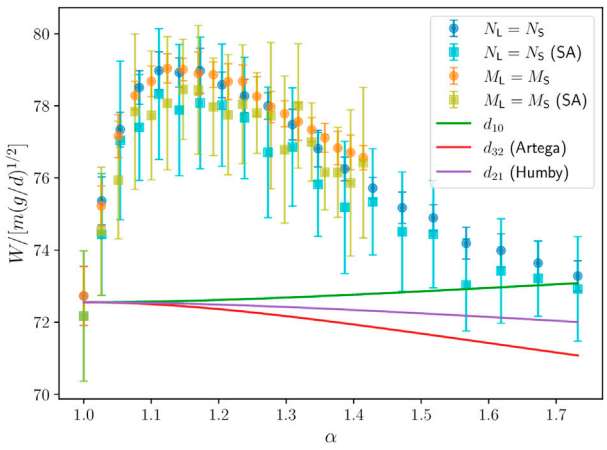

FIGURE 7
Total flow rate W as a function of α for Case I ($N_L = N_S$) and Case II ($M_L = M_S$). Error bars correspond to the standard deviation over 20 realizations of each mixture. The flow rate is calculated both via the slope in Figure 6 (circles) and via the spatial analysis (SA) of density and velocity profiles in Figure 10 (squares). Solid lines correspond to the Beverloo equation corrected by setting the mean particle diameter $\bar{d}$ using various proposed definitions defined in the main text: d_{10}, d_{32} (Artega and Tüzün, 1990), and d_{21} (Humby et al., 1998).

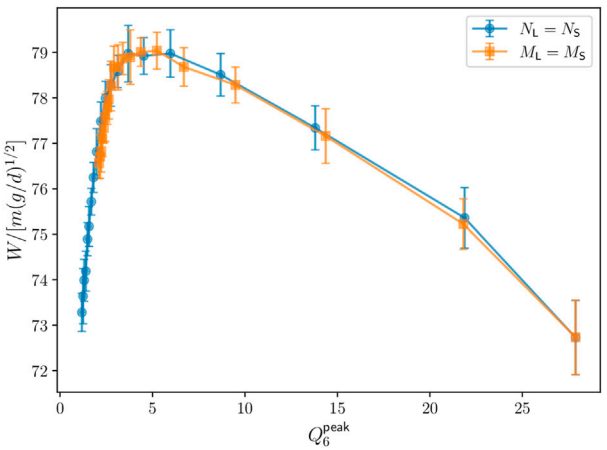

FIGURE 8
Total flow rate W as a function of the descriptor of global order Q_6^{peak} for binary mixtures with same mass ($M_L = M_S$) and same number of grains ($N_L = N_S$) per species.

The Beverloo equation (Eq. 1) can be used to estimate the flow rate of a mixture using $\bar{d}$ as the mean particle diameter of the mixture (Artega and Tüzün, 1990; Humby et al., 1998). If we use our definition $\bar{d} = d_{10}$, and provided that all simulations were done with fixed $\bar{d}$, the flow rate predicted by Eq. 1 should be constant with varying α. In practice, our systems have a small variation in $\bar{d}$ as seen in Tables 1, 2. We have plotted W from Eq. 1 in Figure 7 (green solid line) using the exact value of $\bar{d}$ used in the simulations for the given α. Since the curves for Case I and II are indistinguishable, we just show the curve for Case II.) To fit the flow rate for the monosized sample ($\alpha = 1.0$) we set $C = 1.24$ and $k = 2.0$, which is consistent with values reported by others (Aguirre et al., 2010; Goldberg et al., 2015; Tang and Behringer, 2016). As we can see, the predicted flow rate increases mildly due to the small decrease in $\bar{d}$ and does not show a maximum. Therefore, the nonmonotonic variation in flow rate that we observe cannot be attributed to the small variations in $\bar{d}$ in our simulations.

As we mentioned in Section 2, the mean particle size can be defined in many different ways. Artega and Tüzün (1990) used a volume (area in 2D) weighted definition $\bar{d}_{\text{Artega}} = d_{32} = (N_L d^3_L + N_S d^3_S)/(N_L d^2_L + N_S d^2_S)$. Later, Humby et al. (1998) found that a more accurate prediction of the experimental flow rate is achieved using an area (perimeter in 2D) weighted definition $\bar{d}_{\text{Humby}} = d_{21} = (N_L d^2_L + N_S d^2_S)/(N_L d_L + N_S d_S)$. We have plotted the flow rate predicted by the Artega and Humby definitions of $\bar{d}$ in Figure 7 considering the actual simulated mixtures using the same values of C and k as above. Again, the nonmonotonic behavior observed in the simulations is not predicted by the Beverloo equation given any of these definitions of $\bar{d}$. This implies that the variations in flow rate cannot be simply attributed to changes to the mean particle size of any form (i.e., number, area, or perimeter weighted mean value).

Figure 8 depicts the flow rate as a function of the global hexagonal order Q_6^{peak} of the system. In this plot it becomes more clear that the most hexagonally ordered system (the monosized one) yields, within fluctuations, the same W as the system with almost nonexistent hexagonal order. The maximum flow rate corresponds to the binary mixture with the Q_6 distribution highlighted in Figure 4. After Q_6^{peak} drops below ≈ 4.0, configurations other than the hexagonal arrangement become more frequent. This prevalence of less ordered configurations corresponds with a minor, though clearly discernible, reduction in the flow rate of $\approx 8\%$. In principle, one may be tempted to conclude that a monosized system of disks is inappropriate to model the flow rate of a realistic system because diminishing the degree of hexagonal order leads to a slightly higher flow rate. However, as we observe, when size dispersion is increased beyond $\alpha > 1.5$ the system yields indistinguishable flow rates from that of the monosized system. Hence, the use of a binary mixture with a small size dispersion ($1 < \alpha < 1.5$), although reducing hexagonal ordering, leads to flow rates that depend on α. A monosized system seems to be a reasonable model for a mixture with larger size dispersion. Of course, the nonmonotonic flow rate may be the result of competing mechanisms, and we cannot make a prediction for $\alpha > 2$. To consider the possible competing mechanism we study density and velocity profiles at the orifice in the next section.

Before proceeding, we note here that we do not observe segregation during discharge as we vary the dispersity of the system. As a demonstration, in the insets to Figure 6, we show the instantaneous ratio between the discharged mass of each species (M_L/M_S) as a function of time for the largest α simulated in each case. As we can see, this ratio remains constant, albeit fluctuating, during the simulation.

3.3 Spatial analysis: packing fraction and velocity profiles along orifice

In order to investigate the origin of the small effect on flow rate caused by size dispersion in binary systems, we have measured the packing fraction $\phi(x)$ and vertical velocity $v_\perp(x)$ profile at the plane of the orifice. For a continuum, the mass flow rate is calculated from the integral

$$W = \rho \int_{-D/2}^{D/2} \phi(x) v_\perp(x) dx, \tag{3}$$

where ρ is the 2D material density of the particles. To estimate W from simulation data, we measure packing fraction and velocity profiles along the orifice and carry out a discrete summation.

The packing fraction and velocity profiles at the orifice are obtained from a series of snapshots saved during the simulations (as described in Section 2) which contain the particle positions and velocities. The orifice cross-section is binned in rectangles $d/2$-wide and $d/2$-tall, with the top edge of each bin along the orifice plane, as depicted in Figure 9. The packing fraction in each bin in a single snapshot is determined as the area occupied by grains that overlap with the bin divided by the area of the bin. The average packing fraction in a given bin is then computed across all snapshots. The velocity of grains in each bin in a single snapshot is determined by averaging the velocities of any grains that intersect with the bin area. Then, as with packing fraction, the average velocity vector for the steady state flow is computed across snapshots. We note that the mass flow rate obtained using this method will depend on the height of the sampling box and its vertical position with respect to the orifice. If the bins fall *within* the silo area, not all of the flow rate in the plane at the bottom of the silo is captured.

Figure 7 serves as a validation that the flow rate extracted from the profiles coincides with that obtained from the count of particles crossing the orifice line over time. From Figures 10A, C it is apparent that the packing fraction profile is not affected by α nor the mix rate used (see also Figure 10E). Indeed, the main difference caused by the size dispersion is variation in the velocity profiles (Figures 10B, D). The velocity profile conserves its functional form as α grows, but the maximum velocity (at the center of the outlet) varies (see Figure 10F) in the same proportion as the flow rate (cf. Figure 7). This observation is consistent with previous studies that show a stronger change in particle velocity at the orifice than in packing fraction as the composition of a binary mixture is varied, even with non-constant $\bar{d}$ (Zhou et al., 2015).

A constant packing fraction profile at the orifice plane is a strong indication that some intuitive predictions for mixed particle sizes are unwarranted. A mix of particle sizes tends to produce higher packing fractions in the bulk (Artega and Tüzün, 1990). Naturally, this may mislead us to expect a higher flow rate. However, Figures 10A, C clearly show that the relevant packing fraction that defines flow rate, i.e., that measured at the orifice plane, is in fact unaffected.

Currently, we cannot offer a plausible mechanism for the nonmonotonic variation of the particle velocities at the outlet with size ratio α. However, we argue that this cannot be related with hexagonal ordering in the bulk. The particle velocities at the orifice–a region were the material is dilated–are likely *not* determined by the existence or lack of ordering in the bulk of the container.

3.4 Small orifice size

The results shown in the preceding sections correspond to discharges through an orifice of size $D = 16.9d$, large enough to be well beyond the clogging regime. To assess if our main observations hold for small orifices, we have run simulations for Case I using the smallest orifice for which we observed steady-state flow without clogging across all α: $D = 7.3d$. In Figure 11A, we show the PDF of Q_6 for each α during the steady state. The trends observed for the larger orifice are also present here, though we do observe a smaller height of the main peak for the monosized case in comparison with the larger orifice. As observed in the snapshot displayed in the inset to Figure 11A, this smaller peak seems to be associated with a large number of small, ordered regions with boundary defects in-between. The flow through larger orifices is likely to help "anneal" these defects and increase the size of the ordered domains. However, detailed study of these domains is beyond the scope of the current work.

We plot the flow rate through the small orifice as a function of α in Figure 11B. As for the large orifice, the flow rate is nonmonotonic and presents a maximum at $\alpha \approx 1.15$. Again, the difference between the maximum flow rate and the monosized case is around 8%, and for larger values of α the flow rate is indistinguishable from the monosized system. Therefore all of the features presented in this

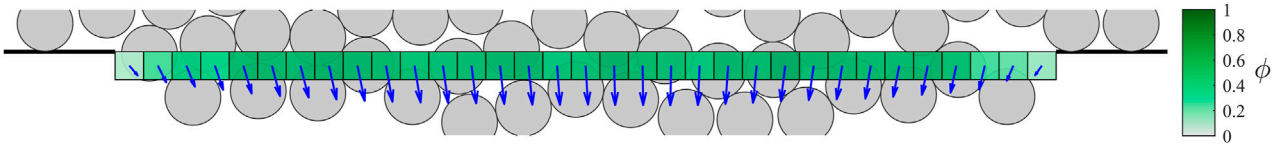

FIGURE 9
Sample diagram of the binning used to calculate the velocity and packing fraction profiles through spatial analysis. The blue vectors correspond to the average velocity in a bin for a single simulation realization; shading of the bin indicates the average packing fraction for a single realization.

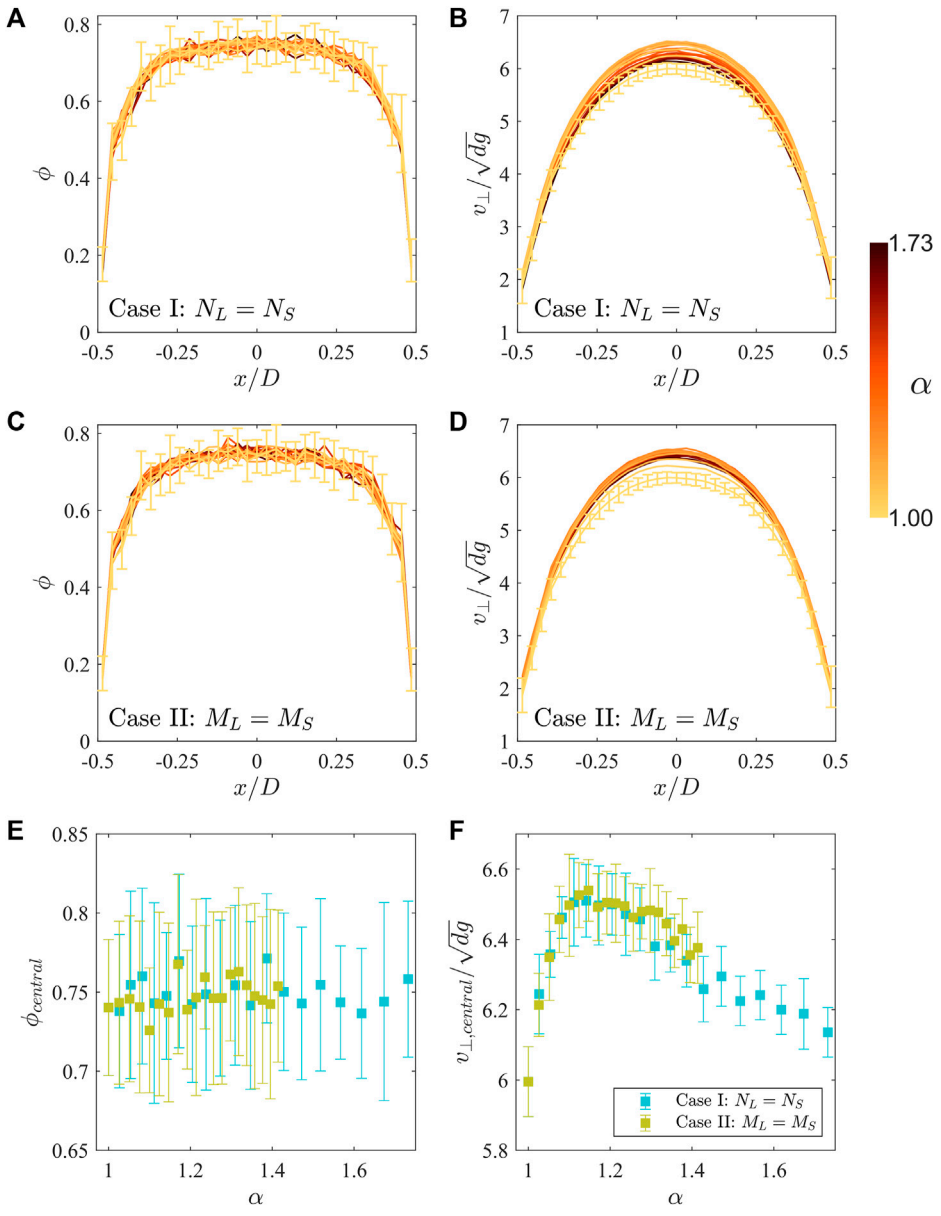

FIGURE 10
Spatial analysis profiles across the silo orifice of the packing fraction **(A,C)** and the vertical velocity **(B,D)** in Cases I and II. Error bars, computed as the standard deviation across all 20 realizations per condition, are shown for the $\alpha = 1$ profiles and are representative of the scale of error bars on the other profiles. **(E,F)** show the packing fraction and vertical velocity at the center of the orifice profile as a function of α; error bars denote standard deviation across realizations.

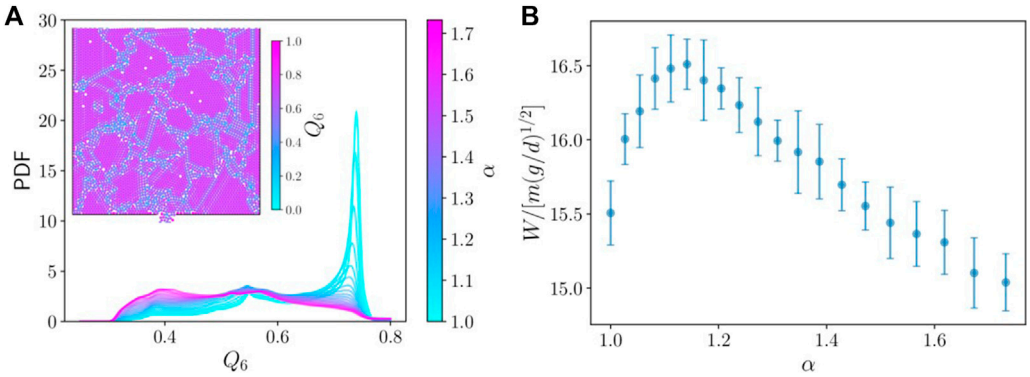

FIGURE 11
(A) PDF of Q_6 for mixtures with $N_L = N_S$ (Case I) with $D = 7.3d$ for varying α (see color scale). Inset: Snapshot during the discharge of a monosized sample. Particles are colored according to their Q_6 bond order parameters. **(B)** Total flow rate W as a function of α for Case I. Error bars correspond to the standard deviation over 20 realizations of each mixture.

work for a larger orifice hold even for a small orifice near the clogging regime.

4 Conclusion

We have simulated 2D binary systems of granular disks discharging through an orifice at the bottom of a silo. We have prepared systems with a fixed (number weighted or mass weighted) mean particle diameter. Bidisperse systems can prevent the formation of hexagonal order regions in 2D systems. However, the flow rate is only partially affected. Some binary mixtures (with a little hexagonal order) present up to 8% higher flow rates. Interestingly, other mixtures with no hexagonal order display the same flow rate as a monosized system that presents highly ordered domains. These observations are valid, both for large and small orifices.

The small change in flow rate when varying size ratio seems to be entirely due to a change in the velocity of the flow rather than different packing fractions at the orifice. For a static sample, when a monosized system is replaced by a bidisperse mixture, one expects an increase in packing fraction. However, the packing fraction of a granular material flowing through a constriction does not need to follow this rule. Since the local packing fraction at the orifice is not correlated with ordering in the bulk, we argue that changes in the flow rate, which are only explained by particle velocities, are not likely to be correlated with ordering that is observed away from the outlet. Our results suggest that, for some purposes, using a monosized system of grains that displays clear ordering may be as representative of a realistic system as a mixture that shows no obvious ordering.

Data availability statement

The raw data supporting the conclusion of this article will be made available by the authors, without undue reservation.

Author contributions

MC: Conceptualization, Formal Analysis, Funding acquisition, Investigation, Methodology, Software, Writing–original draft, Writing–review and editing. RK: Conceptualization, Formal Analysis, Funding acquisition, Software, Writing–original draft, Writing–review and editing. LP: Conceptualization, Formal Analysis, Funding acquisition, Writing–original draft, Writing–review and editing.

Funding

The author(s) declare that financial support was received for the research, authorship, and/or publication of this article. This work was partially funded by CONICET (Argentina) through grant PIP-717 and UNLPam (grant F65). MC is thankful for the financial support from CONICET (Grant No. PUE 2018 229 20180100010 CO) and UTN (Grant No. MAUTILP0007746TC). RK thanks College of the Holy Cross for financial support.

Acknowledgments

We are indebted to Douglas J. Durian for valuable discussions during the course of this research.

Conflict of interest

The authors declare that the research was conducted in the absence of any commercial or financial relationships that could be construed as a potential conflict of interest.

The author(s) declared that they were an editorial board member of Frontiers, at the time of submission. This had no impact on the peer review process and the final decision.

Publisher's note

References

Aguirre, M. A., Grande, J. G., Calvo, A., Pugnaloni, L. A., and Géminard, J. C. (2010). Pressure independence of granular flow through an aperture. *Phys. Rev. Lett.* 104, 238002. doi:10.1103/physrevlett.104.238002

Allen, T. (2013). *Particle size measurement*. Berlin, Germany: Springer.

An, X., Yang, R., Dong, K., and Yu, A. (2011). Dem study of crystallization of monosized spheres under mechanical vibrations. *Comput. Phys. Commun.* 182, 1989–1994. doi:10.1016/j.cpc.2011.02.006

Anyam, V. K. R., and Anki Reddy, K. (2022). Granular mixtures discharging through a silo with lateral orifice. *Phys. Fluids* 34. doi:10.1063/5.0086936

Artega, P., and Tüzün, U. (1990). Flow of binary mixtures of equal-density granules in hoppers—size segregation, flowing density and discharge rates. *Chem. Eng. Sci.* 45, 205–223. doi:10.1016/0009-2509(90)87093-8

Ashour, A., Trittel, T., Börzsönyi, T., and Stannarius, R. (2017). Silo outflow of soft frictionless spheres. *Phys. Rev. Fluids* 2, 123302. doi:10.1103/physrevfluids.2.123302

Benyamine, M., Djermane, M., Dalloz-Dubrujeaud, B., and Aussillous, P. (2014). Discharge flow of a bidisperse granular media from a silo. *Phys. Rev. E* 90, 032201. doi:10.1103/physreve.90.032201

Beverloo, W., Leniger, H., and van de Velde, J. (1961). The flow of granular solids through orifices. *Chem. Eng. Sci.* 15, 260–269. doi:10.1016/0009-2509(61)85030-6

Börzsönyi, T., Somfai, E., Szabó, B., Wegner, S., Mier, P., Rose, G., et al. (2016). Packing, alignment and flow of shape-anisotropic grains in a 3d silo experiment. *New J. Phys.* 18, 093017. doi:10.1088/1367-2630/18/9/093017

Carlevaro, C., and Pugnaloni, L. (2011). Steady state of tapped granular polygons. *J. Stat. Mech. Theory Exp.* 11, 01007. doi:10.1088/1742-5468/2011/01/P01007

Carlevaro, C. M., Kozlowski, R., Pugnaloni, L. A., Zheng, H., Socolar, J. E. S., and Kondic, L. (2020). Intruder in a two-dimensional granular system: effects of dynamic and static basal friction on stick-slip and clogging dynamics. *Phys. Rev. E* 101, 012909. doi:10.1103/PhysRevE.101.012909

Catto, E. (2005). Iterative dynamics with temporal coherence. Available at: https://box2d.org/publications/.

Cervantes-Álvarez, A., Pacheco-Martínez, H., Acosta, C., and Carvente, O. (2023). Dynamics of a 2d silo discharge: a competition between structural domains before clogging. *Phys. A Stat. Mech. its Appl.* 619, 128729. doi:10.1016/j.physa.2023.128729

Dickinson, E., Milne, S., and Patel, M. (1989). Ordering in simulated packed beds formed from binary mixtures of particles in two dimensions: implications for ceramic processing. *Powder Technol.* 59, 11–24. doi:10.1016/0032-5910(89)80091-9

Gao, Q. Q., Chen, Y. C., and Hu, L. (2023). Effect of particle shape on packing fraction and velocity profiles at outlet of a silo. *Chin. Phys. B* 32, 064702. doi:10.1088/1674-1056/aca204

Geng, J., Reydellet, G., Clément, E., and Behringer, R. (2003). Green's function measurements of force transmission in 2D granular materials. *Phys. D. Nonlinear Phenom.* 182, 274–303. doi:10.1016/S0167-2789(03)00137-4

Goldberg, E., Carlevaro, C. M., and Pugnaloni, L. A. (2015). Flow rate of polygonal grains through a bottleneck: interplay between shape and size. *Pap. Phys.* 7, 070016. doi:10.4279/pip.070016

Gray, JMNT (2018). Particle segregation in dense granular flows. *Annu. Rev. Fluid Mech.* 50, 407–433. doi:10.1146/annurev-fluid-122316-045201

Grindlay, J., and Opie, A. (1995). Contact force distribution in a pile of rigid disks. *Phys. Rev. E* 51, 718–723. doi:10.1103/physreve.51.718

Humby, S., Tüzün, U., and Yu, A. (1998). Prediction of hopper discharge rates of binary granular mixtures. *Chem. Eng. Sci.* 53, 483–494. doi:10.1016/s0009-2509(97)00326-6

Jacobs-Capdeville, P., Kuang, S., Gan, J., and Yu, A. (2023). Micromechanical analysis of granular dynamics and energy dissipation during hopper discharging of polydisperse particles. *Powder Technol.* 422, 118462. doi:10.1016/j.powtec.2023.118462

Langston, P. A., Tüzün, U., and Heyes, D. M. (1995). Discrete element simulation of granular flow in 2d and 3d hoppers: dependence of discharge rate and wall stress on particle interactions. *Chem. Eng. Sci.* 50, 967–987. doi:10.1016/0009-2509(94)00467-6

Liu, S., Zhou, Z., Zou, R., Pinson, D., and Yu, A. (2014). Flow characteristics and discharge rate of ellipsoidal particles in a flat bottom hopper. *Powder Technol.* 253, 70–79. doi:10.1016/j.powtec.2013.11.001

Madrid, M., Asencio, K., and Maza, D. (2017). Silo discharge of binary granular mixtures. *Phys. Rev. E* 96, 022904. doi:10.1103/physreve.96.022904

Mankoc, C., Janda, A., Arevalo, R., Pastor, J., Zuriguel, I., Garcimartín, A., et al. (2007). The flow rate of granular materials through an orifice. *Granul. Matter* 9, 407–414. doi:10.1007/s10035-007-0062-2

Moreau, J. J. (1988). "Unilateral contact and dry friction in finite freedom dynamics," in *Nonsmooth mechanics and applications* (Berlin, Germany: Springer), 1–82.

Pongó, T., Fan, B., Hernández-Delfin, D., Török, J., Stannarius, R., Hidalgo, R. C., et al. (2022). The role of the particle aspect ratio in the discharge of a narrow silo. *New J. Phys.* 24, 103036. doi:10.1088/1367-2630/ac9923

Pytlos, M., Gilbert, M., and Smith, C. C. (2015). Modelling granular soil behaviour using a physics engine. *Géotechnique Lett.* 5, 243–249. doi:10.1680/jgele.15.00067

Radjaï, F., Jean, M., Moreau, J. J., and Roux, S. (1996). Force distributions in dense two-dimensional granular systems. *Phys. Rev. Lett.* 77, 274–277. doi:10.1103/PhysRevLett.77.274

Reddy, A. V. K., Kumar, S., and Reddy, K. A. (2021). Granular particle-shape heterogeneous mixtures discharging through a silo. *J. Fluid Mech.* 912, A22. doi:10.1017/jfm.2020.1071

Sakaguchi, H., Ozaki, E., and Igarashi, T. (1993). Plugging of the flow of granular materials during the discharge from a silo. *Int. J. Mod. Phys. B* 7, 1949–1963. doi:10.1142/s0217979293002705

Sands, D. J. (2000). "Powders, and grains: an introduction to the physics of granular materials," in *Partially ordered systems* (New York: Springer-Veriag).

Steinhardt, P. J., Nelson, D. R., and Ronchetti, M. (1983). Bond-orientational order in liquids and glasses. *Phys. Rev. B* 28, 784–805. doi:10.1103/physrevb.28.784

Tang, J., and Behringer, R. P. (2016). Orientation, flow, and clogging in a two-dimensional hopper: ellipses vs. disks. *Europhys. Lett.* 114, 34002. doi:10.1209/0295-5075/114/34002

Tsuchikusa, K., Yamamoto, K., Katsura, M., de Paula, C., Modesto, J., Dorbolo, S., et al. (2023). Disordering two-dimensional magnet-particle configurations using bidispersity. *J. Chem. Phys.* 158, 214501. doi:10.1063/5.0149803

Zhou, Y., Ruyer, P., and Aussillous, P. (2015). Discharge flow of a bidisperse granular media from a silo: discrete particle simulations. *Phys. Rev. E* 92, 062204. doi:10.1103/physreve.92.062204